fault resolution and clarity and the ability to map events across these faults. Fig. 3, *a* shows that the structural elements after Kirchhoff prestack depth migration (PSDM) are more pronounced than those after Kirchhoff poststack time migration (postSTM). In Fig. 3, *b*, a zoomed portion of the left-hand side, demonstrates that an axial-parallel small-scale fault on the crest of the main domal uplift of the structure can be identified and tracked much more confidently after PSDM than after postSTM

The seismic data interpretation workflow utilized and some results of reservoir characterization in this thrust zone are described in [Tiapkina et al., 2010]. The results of reservoir delineation and reservoir description allowed the drilling plans for new exploratory and development wells to be refined.

References

Tiapkina O., Voitsytski Z., Khoma R. Seismic depth imaging in onshore and offshore Ukraine — Case studies // 68th EAGE Conf., Extended Abst. — 2006. — P. 175.

Tiapkina O., Voitsytski Z., Sydorenko G., Parkhomenko T. Imaging and mapping of hydrocarbon traps in areas of complex salt tectonics in Ukraine — Case studies // 70th EAGE Conf., Extended Abst. — 2008. — P. 076.

Tiapkina O., Solovyov I., Polunin O. Imaging and mapping of hydrocarbon traps in a thrust zone from onshore Ukraine — A case study // 72nd EAGE Conf., Extended Abst. — 2010. — P. 312.

Heat flow pattern and fault structures in Donbas

© ***O. Usenko, 2010***

Institute of Geophysics, National Academy of Sciences of Ukraine, Kiev, Ukraine
tectonos@igph.kiev.ua

A map showing the heat flow pattern at depth in Donbas is based on the data of heat flow measurements in over 5000 boreholes(Fig. 1). An unprecedented degree of detail has been achieved making

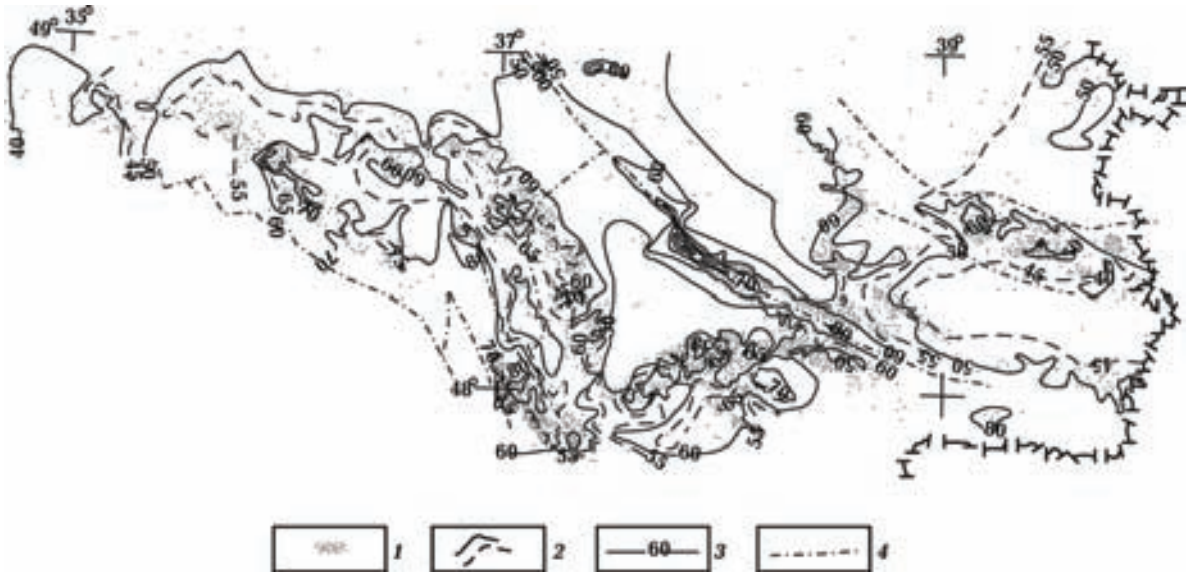

Fig. 1. A map of a heat flow (HF) of Donbas: *1* — points of definition HF; *2* — isolines HF; *3* — values HF (in Mw/m), *4* — fault zone.

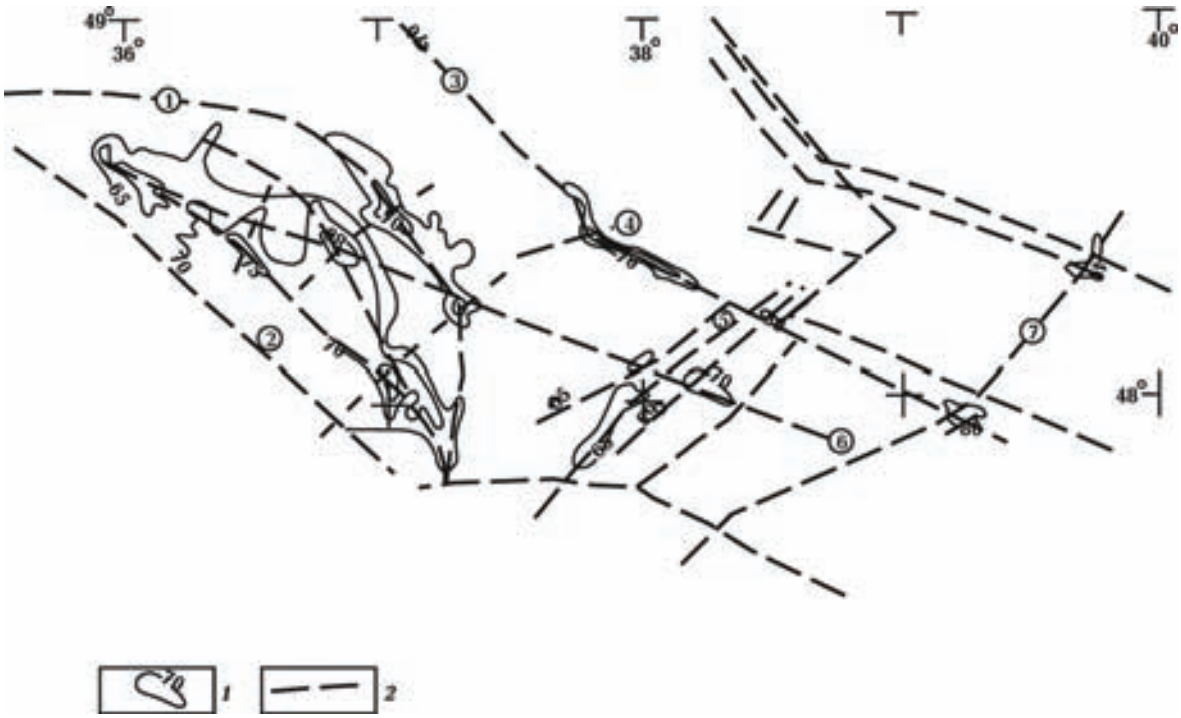

Fig. 2. The scheme of faults of the crystal base and anomalies HF: *1* — anomalies HF: positive, negative; *2* — faults of the crystal base. Figures in circles: *1* — Krivorozhsko-Pavlovskiy; *2* — Southern Donbasskiy; *3* — Axial; *4* — Mikhaylovsko-Yuryevskiy; *5* — Volnovakhsko-Chernukhkhinskiy; axial: *6* — Mushketovsko-Persianovkiy; *7* — Yelanchik-Rovenkovskiy.

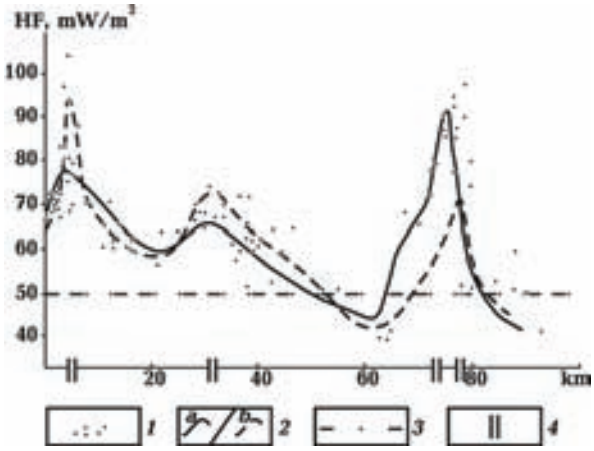

Fig. 3. HF along line AB: *1* — values HF by results of individual definitions; *2* — values HF on isolines: (*a* — in 2 km to the northwest, *b* — in 2 km to the southeast from a line AB); *3* — background values HF; *4* — faults of the crystal base.

it possible to draw maps to the scale of 1:200 000 for the entire region and 1:50 000—1:25 000 for individual areas.

Heat flow values have been calculated as a function of the average geothcrmal gradient between the surface and the borehole face (the temperature at the surface is assumed to be 10 °C) and the thermal conductivity of rocks there 1.65—2.6 W/mK.

The values of temperatures at the borehole faces were adjusted to allow for palcoclimatic variations. The effect of long-term climatic changes in the case of 1000—1400 m deep boreholes takes the form of a 2.9—3.2 °C decrease in the temperature observed at the borehole face. For the Main and Druzhkovsko-Konstantinovskaya anticlines we had to introduce a structural adjustment of –7 mW/m^2 at the curve of the fold, –4 mW/m^2 at the limb, with a gentle increase to +1 mW/m^2 at the transition to the Bakhmutskaya and Kalmius-Toretskaya troughs. In view of the fact that heat flow values were determined based on the temperatures measured at the faces of the boreholes going down to depths over 1000 meters, no hydrogeological adjustment was introduced because earlier studies had not revealed in the region at those depths any appreciable effect of the downpouring waters.

The territory is largely characterized by heat flow values ranging from 42 to 52 mW/nr (the Kalmius-Toretskaya and Bakhmutskaya troughs and the ter-

ritory north of the Nagolnyy Range to the Northern zone of fine folding). In the Northern fine folding zone the heat flow rises to 48—55 mW/m^2, further increases to 62 mW/m^2 at the junction with the Bakhmutskaya Trough, and amounts to 52—56 mW/ra^2 at the slope of the Voronezh block. Maximum heat flow values have been found at the slope of the Ukrainian Shield as well as in the areas of the Main and Druzhkovsko-Konstantinovskaya anticlines in the Donctsk-Makeyevka area. Average heat flow vc.iucs there amount to 63, maximum values reach 75 in the Donetsk-Makeyevka area, 103 at the slope of the Ukrainian Shield, and 104 mW/m^2 in the Nikitovskiy ore field confined to the Main anticline.

The most common heat flow values — 48 mW/m^2 — encountered in the area have been adopted as background values. The derived result is not much higher than the calculated or observed background heat flow in the Ukrainian Shield or Voronezh block (about 45 mW/m^2).

Virtually everywhere the anomalies stretch along the major folded structures of the basin and are quite extensive in length (up to 140 km) but not in width (4—10 to 20 km). They separate areas with relatively low heat flow values. Narrow anomalies correspond to deep-seated longitudinal faults, while background values are typical of blocks undisturbed by faulting. That the anomalies are associated with none other than location of fault zones (rather than folded structures) is clearly displayed in the southwestern part of Donbas (Fig. 2). Higher heat flow values there are confined to the intersection of the Mikhaylovsko-Yuryevskiy and Volnovakhsko-Chernukhkhinskiy faults rather than to the Volchanskaya syncline, whose axis intersects the anomaly at the 45 degrees angle. Heat flow highs mark the intersection of transverse and longitudival faults.

Quite intensive anomalies have been revealed at the southwestern edge of the basis. They run from northwest southeastwards above the Southern part of Donbass, Krivorozhsko-Pavlovskiy, and Mikhaylovsko-Yuryevskiy faults within the crystalline basement. Areas between closely spaced fault zones are characterized by heat flow values higher than background ones (56—58 mW/m^2), but immediately above the fault zones the heat flow values increase sharply (to 104 mW/m^2).

The diagram (Fig. 3) shows a profile of heat flow values measured within a 4 km — wide "corridor". Solid and dashed lines mark heat flow isolines (at the northern and southern borders of the "corridor," respectively). Dots show results of individual measurements. The diagram proves that the scatter of heat flow values is not due to an error in the heat flow determination but to variations in the thermal field intensity. There is no doubt whatsoever that the heat flow highs are confined to zones within the sedimentary layer above faults in the basement. A displacement of the Axial fault zone between the Main and Druzhkovsko-Konstantinovskaya anticlines is responsible for the displacement of the heat flow high. Sharp increases in the intensity have been noted over the entire length of the Mushketovsko-Persianovkiy (up to 85 mW/m^2) and Axial (up to 104 mW/m^2) faults. The northern fault zone is marked by insignificant (up to 55 mW/m) heat flow hikes.

The detailed determinations of heat flow values makes it abundantly clear that some of the faults are represented by up to 20 km wide zones (Southern Donbasskaya, Volnovakhsko-Chernukhinskaya. and others).

The Ukrainian Shield slope is cut by a network of closely spaced transverse and longitudinal faults, and this enables one to concur with geologists who view it as one integral zone. The heat flow map also reveals a displacement of the Volnovakhsko-Chernukhinskiy fault at the intersection of the longitudinal Mushketovsko-Persianovskiy and Axial faults that these authors have also noted. A displacement of the Axial fault at the transition from the Main to the Druzhkovsko-Konstantinovskaya anticline is obvious.

Thus, vertical movements of blocks, as indicated by the present level of erosion shear, were not the only type of displacement during previous episodes of intensification of the deep-seated processes. Horizontal movements with an amplitude of displacement of up to 10—15 km also took place. The currently observed elevated heat flow values associated with the efflux of heat and fluids (including hydrocarbons) are not the only indication of the existence of fault zones and their intersections. The presence of such structures is also indicated by magmatism, hydrothermal ore mineralization (gold, mercury and so on) left by past intensification episodes. One can observe at the intersection of the fault zones an abrupt change in the lithification of sedimentary rocks (including coal) as a result of changes in the level of the erosion shear in different blocks of the crystalline basement. It is therefore an important task to look for fault zones when prospecting for minerals. This task can be tackled with the help of detailed heat-flow maps. On territories involved in recent deep-seated processes, such faults can be pinpointed by hikes in the heat flow values. In the absence of recent intensification processes or of heat emanating from the depth, fault zones are marked by insignificant (up to 5 mW/m) negative heat flow anomalies (the northern part of the Yelanchik-Rovenkovskiy fault).

A fundamental possibility of identifying faults on

the basis of variations in the heat flow values has been demonstrated in the southwestern part of the region where anomalies trace the extension of the faults through the slope of the Ukrainian Shield.

Modeling of the nonlinear resonant response in sedimentary rocks

© V. Vakhnenko[1], O. Vakhnenko[2], J. TenCate[3], T. Shankland[3], 2010

[1]Institute of Geophysics, National Academy of Sciences of Ukraine, Kiev, Ukraine
vakhnenko@ukr.net
[2]Institute for Theoretical Physics, National Academy of Sciences of Ukraine, Kiev, Ukraine
vakhnenko@bitp.kiev.ua
[3]Los Alamos National Laboratory, New Mexico, USA
tencate@lanl.gov
shankland@lanl.gov

Sedimentary rocks, particularly sandstones, are distinguished by their grain structure in which each grain is much harder than the intergrain cementation material [Guyer, Johnson, 1999]. The peculiarities of grain and pore structures give rise to a variety of remarkable nonlinear mechanical properties demonstrated by rocks, both at quasistatic and alternating dynamic loading [Guyer, Johnson, 1999; TenCate, Shankland, 1996; TenCate et al., 2000; Darling et al., 2004]. We suggest a model for describing a wide class of nonlinear and hysteretic effects in sedimentary rocks at longitudinal bar resonance. In particular, we explain: hysteretic behaviour of a resonance curve on both its upward and downward slopes; linear softening of resonant frequency with increase of driving level; gradual (almost logarithmic) recovery of resonant frequency after large dynamical strains; and temporal relaxation of response amplitude at fixed frequency. Starting with a suggested model, we predict the dynamical realization of end-point memory in resonating bar experiments with a cyclic frequency protocol. These theoretical findings were confirmed experimentally at Los Alamos National Laboratory.

A reliable probing method widely applied in resonant bar experiments is to drive a horizontally suspended cylindrical sample with a piezoelectric force transducer cemented between one end of the sample and a massive backload, and to simultaneously measure the sample response with a low-mass accelerometer attached to the opposite end of the bar[2,4]. The evolution equation for the field of bar longitudinal displacements u as applied to above experimental configuration we write as follows

$$\rho \frac{\partial^2 u}{\partial t^2} = \frac{\partial \sigma}{\partial x} + \frac{\partial}{\partial x}\left[\frac{\partial \Im}{\partial(\partial^2 u/\partial x \partial t)}\right]. \qquad (1)$$

Here we use the Stokes internal friction associated with the dissipative function $\Im = (\gamma/2)\times$ $\times[\partial^2 u/\partial x \partial t]^2$. The quantities ρ and γ are, respectively, mean density of sandstone and coefficient of internal friction. The stress-strain relation $(\sigma - \partial u/\partial x)$ we adopt in the form

$$\sigma = \frac{E \operatorname{sech}\eta}{(r-a)\,[\cosh\eta\,\partial u/\partial x + 1]^{a+1}} - \frac{E \operatorname{sech}\eta}{(r-a)\,[\cosh\eta\,\partial u/\partial x + 1]^{r+1}}, \qquad (2)$$

which for $r > a > 0$ allows us to suppress the bar compressibility at strain $\partial u/\partial x$ tending toward $+0-\operatorname{sech}\eta$. Thus, the parameter $\operatorname{coch}\eta$ is assigned for a typical distance between the centers of neighboring grains divided by the typical thickness of intergrain cementation contact.

The indirect effect of strain on Young's modulus E, as mediated by the concentration c of ruptured intergrain cohesive bonds, is incorporated in our theory as the main source of all non-trivial phenomena. We introduce a phenomenological relationship between defect concentration and Young's modulus. Intuition suggests that E must be some monotonically decreasing function of c, which can be expanded in a power series with respect to a small deviation of c from its unstrained equilibrium